Available online at www.sciencedirect.com

SciVerse ScienceDirect

Ceramics International 38 (2012) 6815–6822

CERAMICS INTERNATIONAL

www.elsevier.com/locate/ceramint

Preparation of Si–C–N–Fe magnetic ceramic derived from iron-modified polysilazane

Cong Zhou[a,b], Le Yang[a], Hao Geng[a], Qiang Zheng[a], Hao Min[a], Zhaoju Yu[a,*], Haiping Xia[a,b]

[a]*College of Materials, Key Laboratory of High Performance Ceramic Fibers, Ministry of Education, Xiamen University, Xiamen 361005, China*
[b]*College of Chemistry & Chemical Engineering, Xiamen University, Xiamen 361005, China*

Received 19 April 2012; received in revised form 25 May 2012; accepted 25 May 2012
Available online 1 June 2012

Abstract

In this paper, Si–C–N–Fe magnetoceramics were obtained by pyrolysis of iron-modified polysilazane (PFSZ) precursors which were synthesized by using polysilazane (PSZ) and iron (III) acetylacetonate ($Fe(acac)_3$) as starting materials. The as-synthesized PFSZ precursors were characterized by Fourier transform infrared spectroscopy (FT-IR) and gel permeation chromatography. The polymer-to-ceramic conversion of the PFSZ was studied by FT-IR and thermal gravimetric analysis. It is found that the ceramic yield of the PFSZ precursor is ca. 25% higher than that of the original PSZ. The crystallization behavior, microstructures and magnetic properties of the PFSZ-derived Si–C–N–Fe magnetoceramics were studied by techniques such as X-ray diffraction, transmission electron microscopy and vibrating sample magnetometer. The results indicate that the formed α-Fe nanoparticles are uniformly dispersed in amorphous Si–C–N(O) matrix, leading to the soft magnetization of the resultant Si–C–N–Fe ceramics. Moreover, the iron content and the magnetic properties of the Si–C–N–Fe ceramic could be easily controlled by the amount of $Fe(acac)_3$ in the precursor.

Keywords: A. Polymer precursors; D. Polymer-to-ceramic conversion; D. Silicon carbide; D. Silicon nitride

1. Introduction

Polymer-derived ceramics (PDCs) such as SiC, Si_3N_4, as well as Si–C–N composite materials, have superior thermostability and mechanical properties [1–4]. The PDC route was almost focused on the design of polymeric precursors for ceramics to emphasize thermal stability and strength of materials [5–7]. Recently, PDCs modified with metallic elements (Fe, Co, Ni, Ti, Zr and Mn) have attracted much interest due to their electrical and magnetic properties [8–18].

PDCs based Si–C–N system have been reported to exhibit extraordinary high temperature properties [1]. The metal-modified Si–C–N ceramics were also studied [19–28]. It is well known that iron has the highest magnetic moment among all three transition metals. The incorporation of iron into Si–C–N ceramics is desirable as it will introduce interesting magnetic properties into the ceramics. Saha et al. [23] reported the synthesis of iron modified Si–C–N ceramics by incorporating Fe_3O_4 into liquid polysilazane (PSZ) and then pyrolyzed up to 1100 °C in a nitrogen atmosphere. The evolution of CH_4 and H_2 reduced the Fe_3O_4 into α-Fe, generating a high-temperature magnetic material for applications in harsh environments. Hauser et al. [24] reported the pyrolytic conversion of a PSZ blended with Fe or $Fe(CO)_5$ in argon to obtain Si–Fe–C–N ceramics, which have a high saturation magnetization of ~57 emu/g and good ferromagnetic behavior. Dumitru et al. [25] reported a versatile method to prepare inorganic polymer precursors by plasma polymerization. The precursors were then converted to Si–C–N–Fe nanostuctured ceramics. Francis et al. [26] studied the crystallization behavior and the controlling mechanism of a Si–Fe–C–N system based on PSZ-derived SiCN ceramic filled with iron metal powder. Xie's group [27] synthesized a hyperbranched PSZ containing iron compound by the polycondensation of silazane lithium salts with $FeCl_3$, then the PSZ was pyrolyzed under nitrogen, argon or NH_3 to obtain a series of magnetic ceramics.

*Corresponding author.
E-mail address: zhaojuyu@xmu.edu.cn (Z. Yu).

0272-8842/$36.00
http://dx.doi.org/10.1016/j.ceramint.2012.05.080

Subsequently, they prepared another iron-containing PSZ by the amine displacement reaction along with heat-induced vinyl crosslinking reactions between Fe[N(Si-$Me_2Vi)_2]_3$ and the PSZ containing $-Si–Vi-$ [28]. The authors suggested that α-Fe was the only magnetic crystalline embedded in the amorphous Si/C/N-based matrix. However, the above mentioned methods have many disadvantages. For instance, mixing iron or iron compounds into PSZ precursors might cause heterogenous dispersion of Fe in the PDC matrix or the processing is difficult to control due to the complex synthesis routes.

In this paper, we try to prepare an iron-modified PSZ by using iron (III) acetylacetonate ($Fe(acac)_3$) as a new source of iron. As expected, the resultant Si–C–N–Fe ceramics show relatively good magnetic properties. Herein, we report the first results about the reactivity of the $Fe(acac)_3$ versus the PSZ and their application to the preparation of the Si–C–N–Fe ceramics.

2. Experimental

2.1. General

All manipulations were carried out by using standard high vacuum or inert atmosphere techniques as described by Shriver and Drezdzon [29]. $Fe(acac)_3$ with a 99% purity was purchased from Alfa Aesar. Dimethylbenzene was distilled from a sodium benzophenone ketyl prior to use. Liquid PSZ with a composition formula $-[SiH(CH_3)NH]_x–[Si(CH=CH_2)(CH_3)NH]_y–[Si(CH_3)(NH)NH]_z-$ was prepared by the ammonolysis reaction of CH_3SiHCl_2, $CH_3Si(CH=CH_2)Cl_2$ and CH_3SiCl_3 [30]. PSZ used in this work had a number-average molecular weight of ca. 500 and a polydispersity index of 1.8.

Fourier transform infrared (FT-IR) spectra were recorded on a Nicolet Avator 360 apparatus (Nicolet, Madison, WI) with KBr plates for liquid samples and KBr disks for solid samples. Gel permeation chromatography (GPC) measurements were performed at 30 °C with tetrahydrofuran as the eluant (1.0 mL/min) by using an Agilent 1100 system (Agilent, Santa Clara). The calculation of the molecular weight of the PSZ was calibrated with narrow polystyrene standards. Thermal analysis for the pyrolytic conversion of the cured PSZ and PFSZs was performed on a thermal gravimetric analysis (TGA, Netzsch STA 409 EP, Germany). X-ray diffraction (XRD, PANalytical, Netherlands) was carried out to study the crystallization behavior with a Cu*Kα* radiation. Iron contents in ceramics were determined by energy disperse spectroscopy (EDS, JAX-8100, Japan). Transmission electron microscopy (TEM, JEM-2100, Japan) was used to observe the microstructure of the ceramics. The magnetic properties were measured by using a vibrating sample magnetometer system (TOEIVSM-5–15, Japan) at room-temperature, and the standard sample is Ni. The Hk was determined by calculating the measured easy axis and hard axis loops of the reduced magnetization.

2.2. Synthesis of precursors

The preparation of iron-modified PSZ (PFSZ) precursors was carried out in a Schlenk flask with a reflux condenser, a magnetic stirrer and an argon inlet. A typical synthesis of the PFSZ was achieved with the following procedure: 0.189 g $Fe(acac)_3$ was introduced into a 150 mL Schlenk flask in an argon atmosphere, and then 20 mL dry dimethylbenzene was added to solve $Fe(acac)_3$ until a clear red solution was obtained. After that, 3 g PSZ was introduced into the Schlenk flask with stirring at room temperature, and this solution was heated up to 140 °C for 6 h under an argon atmosphere. Finally, a viscous red PFSZ precursor was obtained in the flask after the dimethylbenzene was stripped off under vacuum at 100 °C. The weight ratios of Fe to PSZ were 1%, 3% and 5%, and the obtained samples were abbreviated as PFSZ-1, PFSZ-2 and PFSZ-3, correspondingly.

2.3. Curing and pyrolysis

Thermal curing of the PSZ and the PFSZs precursors were carried out in an inert atmosphere, placed in a 180 °C oil bath for 12 h. The liquid PSZ was transformed slowly into a viscous and white colloid, while the PFSZs were cured into red and stiff solids quickly.

The cured samples were put in an alumina boat and thereafter pyrolyzed in a glass silica tube under an argon flow. The pyrolysis temperature was raised up to 900 °C at a rate of 5 °C/min, and then kept at 900 °C for 2 h. To study the crystallization behavior of the ceramics annealed at higher temperatures, the sample (pyrolyzed at 900 °C) was put in a graphite crucible and heated in a tube furnace in an argon atmosphere. The 900 °C ceramic was heated rapidly to 1100 °C, 1200 °C and 1300 °C, at a rate of 40 °C min^{-1} and kept at this temperature for 2 h. After that, the resulting ceramic was furnace-cooled to RT.

3. Results and discussion

3.1. Characterization of PFSZ precursors

The PFSZs were characterized by means of FT-IR (Fig. 1). As previously reported, absorption peaks at 3385 and 1175 cm^{-1}(N–H), 3050 cm^{-1} (C=C–H), 2950 and 2900 cm^{-1}(C–H), 2100 cm^{-1} (Si–H), 1250 cm^{-1} (Si–CH_3) and 1590 cm^{-1} (C=C) are observed [30]. It is worth mentioning that the characteristic absorption peaks at 1521 cm^{-1} (C=C stretching) and 1577 cm^{-1} (C=O stretching) derived from $Fe(acac)_3$ [31] are also observed in the spectra of PFSZs. In comparison with the original PSZ, the Si–H stretch (2100 cm^{-1}) peak of PFSZs decreases. The results suggest that there should be a reaction between $Fe(acac)_3$ and PSZ.

In order to investigate the molecular weight of PFSZ, the original PSZ and the typical PFSZ-1 were subjected to GPC analysis (Fig. 2). It is apparent that the GPC trace of PFSZ-1 exhibits some new high-molecular-weight peaks

compared with that of the PSZ, indicating that chemical reaction between the PSZ and $Fe(acac)_3$ did occur. The GPC results agree well with the FT-IR results.

As regarding the reaction mechanism between PSZ and $Fe(acac)_3$, it should involve the condensation reaction of the Si–H groups from PSZ and the Fe–O groups from $Fe(acac)_3$ (Scheme 1). As previously reported, the reaction of polycarbosilane (PCS) with zirconium (IV) acetylacetonate ($Zr(acac)_4$) proceeds by the condensation reaction of the Si–H bonds in PCS and the ligands of $Zr(acac)_4$ accompanied by the evolution of acetylacetone, resulting in a molecular weight increase based on the formation of Si–Zr bond [32]. The molecular structure of $Fe(acac)_3$ is very similar to that of $Zr(acac)_4$, and the PSZ has abundant Si–H groups. Therefore, the condensation reaction of the Si–H bonds in PSZ and the ligands of $Fe(acac)_3$ should take place, which is supported by the FT-IR and the GPC results. However, it is difficult for all of the three ligands of $Fe(acac)_3$ to execute the condensation reaction because of the steric hindrance, which is confirmed by the finding that characteristic absorption peaks at 1521 cm^{-1} (C=C stretching) and 1577 cm^{-1} (C=O stretching) derived from ligands of $Fe(acac)_3$ remain in the spectra of PFSZs. Even though the reaction between PSZ and $Fe(acac)_3$ seems to be incomplete, the unreacted $Fe(acac)_3$ may further react with PSZ during the followed processes of curing and pyrolysis.

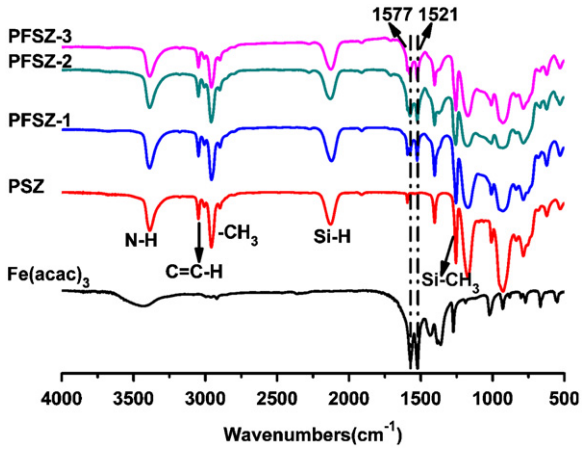

Fig. 1. FT-IR spectra of $Fe(acac)_3$, PSZ and PFSZs.

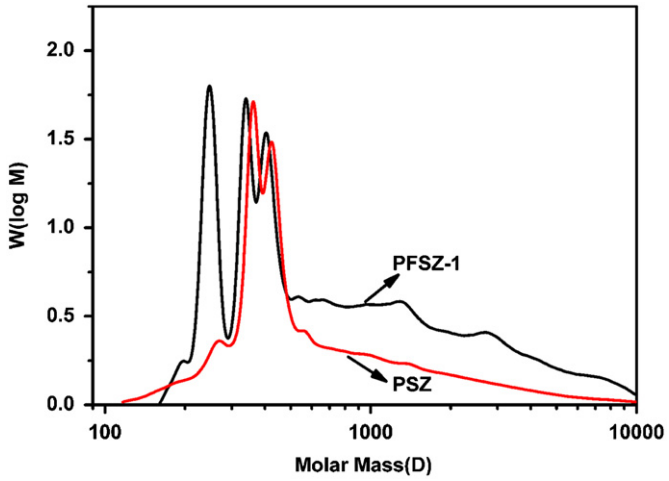

Fig. 2. GPC traces of PSZ and PFSZ-1.

3.2. Curing and ceramization of PFSZs

It is well accepted that ceramic yield of a polymeric precursor could be significantly improved via a previous cross-linking treatment before pyrolysis. In the present work, the as-synthesized PFSZs were thus subjected to heat treatment for cross-linking before high temperature pyrolysis. The cross-linking reactions of the PFSZs and the PSZ were investigated by FT-IR (Fig. 3). When heated at 180 °C for 12 h, the PSZ was slowly transformed into a viscous and white colloid. In contrast, the PFSZs were rapidly cured at 180 °C within 5–10 min. It indictates that the cross-linking of the PFSZ is significantly improved when compared with that of the PSZ, which is supported by the finding that the decrease in intensity of the peak at 2100 cm^{-1} (Si–H) is marked much more for the thermally cross-linked PFSZs than for the PSZ (Fig. 3). The more $Fe(acac)_3$ was introduced into the PFSZs, the more Si-H peak intensity decreased. The results suggest that the remaining Si–H groups of the PFSZs did further react with the Fe–O groups for further cross-linking, as indicated in Scheme 1.

To study the structural evolution during the polymer-to-ceramic conversion, the PFSZ-3 samples heat-treated at different temperatures were characterized by FT-IR. As indicated in Fig. 4, active groups such as N–H, Si–H and C=C still remain in the PFSZs. It is found that the peaks of N–H, Si–H and C=C reduced gradually when the pyrolysis temperature increased from 180 °C to 500 °C, which is due to dehydrogenation coupling and transamination [30]. From 500 °C to 700 °C, the peaks of Si–CH_3 reduced because of the decomposition of organic side groups. It is worth mentioning that the peak at 1577 cm^{-1} attributed to C=O groups in the ligands of

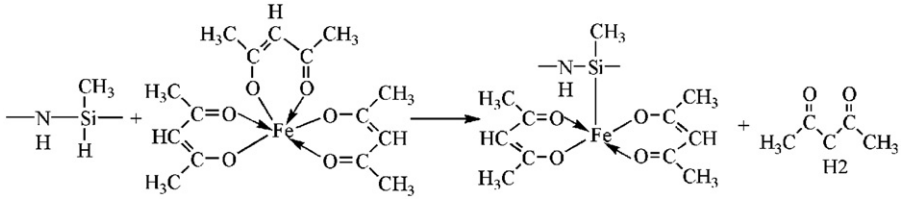

Scheme 1. Synthesis of PFSZ via reaction between PSZ and $Fe(acac)_3$.

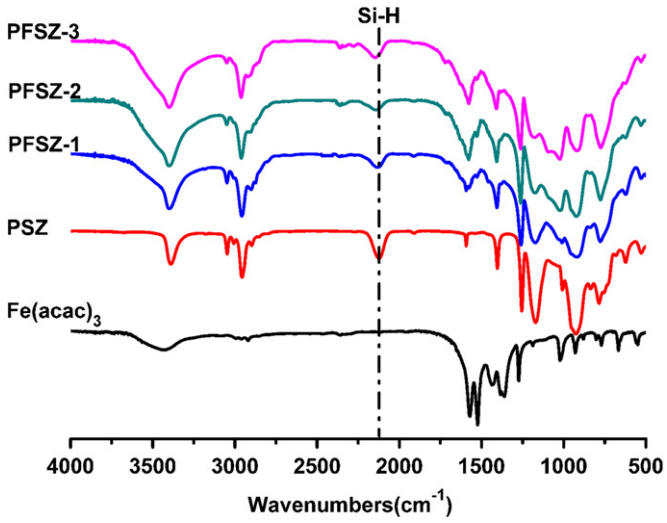

Fig. 3. FT-IR spectra of cured PFSZs and PSZ heated at 180 °C for 12 h.

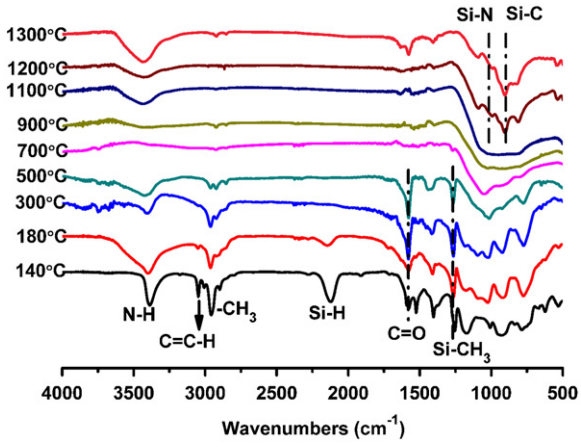

Fig. 4. FT-IR spectra of PFSZ-3 heat-treated at different temperatures.

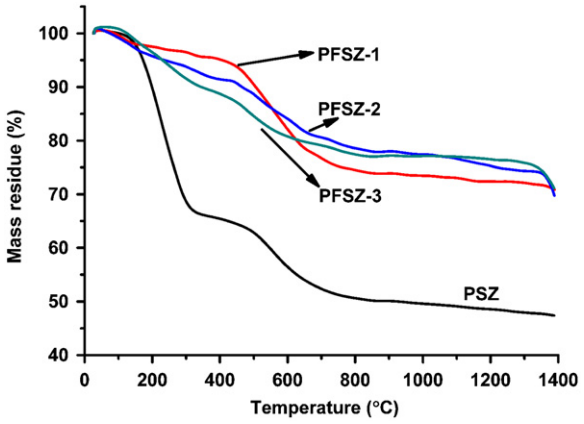

Fig. 5. TGA curves of the cured PFSZs and PSZ.

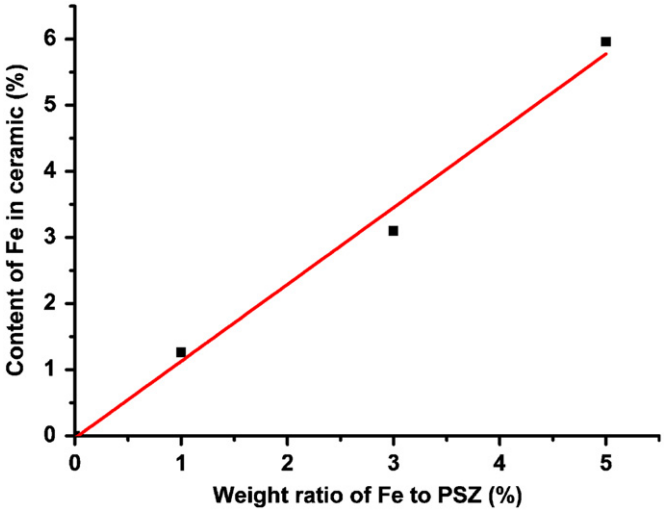

Fig.6. Dependence of Fe contents in 1200 °C ceramics on Fe contents in PFSZs.

$Fe(acac)_3$ vanished at temperatures over 700 °C, indicating the decomposition of the ligands. Only the SiC absorption peak retained at 900 °C; therefore, it is believed that the polymer-to-ceramic conversion is completed at 900 °C. From 1100 °C to 1300 °C, the peaks of Si–C and Si–N become sharper with the increasing temperature, indicating crystallization of SiC and Si_3N_4.

The thermal properties of PFSZs and PSZ were measured by TGA and the results are shown in Fig. 5. For PSZ by 300 °C, the TGA curve shows a mass loss of 30%, much higher than that of PFSZs (5–10%). In the 300–900 °C region, the mass loss of the PFSZs closely matched that of PSZ (about 18%). In the 900–1300 °C region, no obvious weight loss is observed for either the PSZ or the PFSZs, indicating the completion of polymer-to-ceramic conversion. Generally, the 900 °C ceramic yields of the PFSZs range from 75% to 78%, which are about 25% higher than those of the PSZ. The significantly lower mass loss of the PFSZs than that of the PSZ below 300 °C is attributed to the more evaporation of oligomers contained in the PSZ, which is also responsible for the higher final ceramic yield of the PFSZs. The results suggested that the evaporation of the low-molecular-weight oligomers was markedly reduced to improve the final ceramic yield because of the cross-linking reaction. Moreover, slight mass loss occurred from 1300 to 1400 °C for the PFSZ, which might be due to the introduction of oxygen from $Fe(acac)_3$.

The iron contents of the ceramics were calculated from their EDS spectra and the results are shown in Fig. 6. It reveals that the Fe content in the final ceramic increases linearly with the increase in the weight ratio of Fe to PSZ in the feed, indicating that the Fe content in the ceramic could be easily regulated by the amount of $Fe(acac)_3$ in the precursor.

3.3. Microstructure of PFSZ-derived ceramics

To investigate the crystallization behavior of the PFSZ-derived ceramics, XRD patterns of the samples were

measured and the results are shown in Fig. 7. Below 700 °C, the ceramic is amorphous and highly disordered. At 900 °C, a weak peak appears at about 45°, indicating the formation of the α-Fe. With the temperature increasing the peak of the α-Fe becomes sharper, suggesting the increased degree of crystallization. The characteristic peaks of β-SiC appear until 1200 °C with the three major peaks at $2\theta = 36°$, 60°and 72°, accompanied by the peaks of α-Si_3N_4 which are located at $2\theta = 20°$, 23°, 26°, 31°, 34°, and 35°. At 1300 °C, all these peaks become sharper and higher.

In addition, the effect of the iron content in the 1300 °C ceramics on the crystallization behavior was also investigated. The ceramics derived from PSZ, PFSZ-1, PFSZ-2, and PFSZ-3 are presented as Si–C–N, Si–C–N–Fe-1, Si–C–N–Fe-2 and Si–C–N–Fe-3, respectively. Fig. 8 shows that the PSZ-derived Si–C–N ceramic is almost amorphous and disordered. In contrast, the PFSZ-derived Si–C–N–Fe ceramics are partially crystallized. It is also observed that the crystallization of β-SiC and α-Si_3N_4 are improved by the introduction of iron into the Si–C–N–Fe ceramics. According to the literature, crystallization behavior of PSZ derived ceramics was influenced by chemical composition, molecular structure and chemical homogeneity of amorphous Si–C–N network [33]. The introduction of $Fe(acac)_3$ destroyed the chemical homogeneity and reduced the content of N in the precursors, leading to the lower crystallization temperature of PFSZ-derived ceramics than that of the PSZ-derived ceramics [34]. In addition, the intensity of the α-Fe peak gradually increases with the increasing iron content of the ceramic.

In order to study the formation of α-Fe, the pure $Fe(acac)_3$ was pyrolyzed at 900 °C under an argon atmosphere. Fig. 9 depicts the XRD patterns of $Fe(acac)_3$-derived product and the Si–C–N–Fe-3 ceramic. It is observed that the $Fe(acac)_3$-derived product consists of α-Fe and Fe_3O_4. However, the α-Fe is the only crystallization phase and no Fe_3O_4 phase is detected in the Si–C–N–Fe system, which might be due to the carbothermal reduction reaction of Fe_3O_4 in the ceramic matrix. The reaction is as follows.

$$Fe_3O_4 + 4C\ (\text{free carbon}) \rightarrow 3Fe + 4CO$$

To further investigate the iron morphology in the Si–C–N–Fe ceramic, the TEM measurements of the 1200 °C Si–C–N–Fe-3 ceramic were performed and the results are shown in Fig. 10. Fig. 10(a) demonstrates that the PFSZ-3-derived ceramic annealed at 1200 °C consists of SiC and Fe crystallites, with grain sizes in the range 10–30 nm. Fig. 10(b) shows that the Fe particles of 10–20 nm are uniformly dispersed in the amorphous Si–C–N(O) matrix. Fig. 10(c) and (d) reveals that the interplanar spacing of 0.25 nm and 0.20 nm corresponds to the (1 1 1) plane of the β-SiC and (1 1 0) plane of the α-Fe, respectively [14].

The Si_3N_4 crystallites in the 1200 °C Si–C–N–Fe–3 ceramic are too small to be found in Fig. 10, so the TEM measurements of the 1300 °C Si–C–N–Fe-3 ceramic were performed and the images are shown in Fig. 11. Fig. 11(a) demonstrates the bright field lattice image of the 1300 °C ceramic. The crystallites in the 1300 °C ceramic grew up dramatically in comparison with those in the

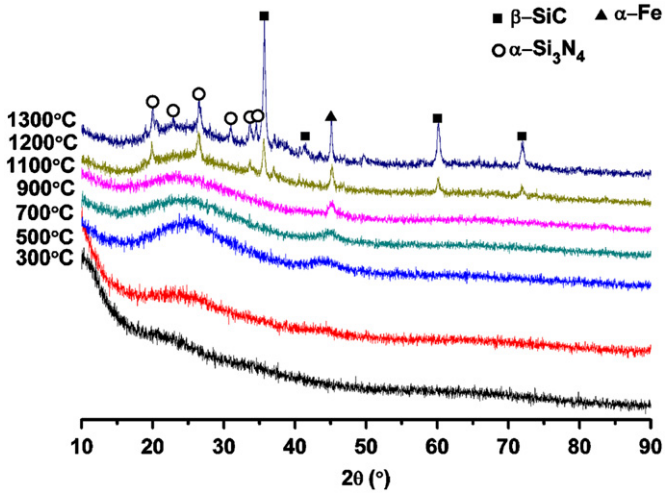

Fig. 7. XRD patterns of PFSZ-3 heat-treated at different temperatures.

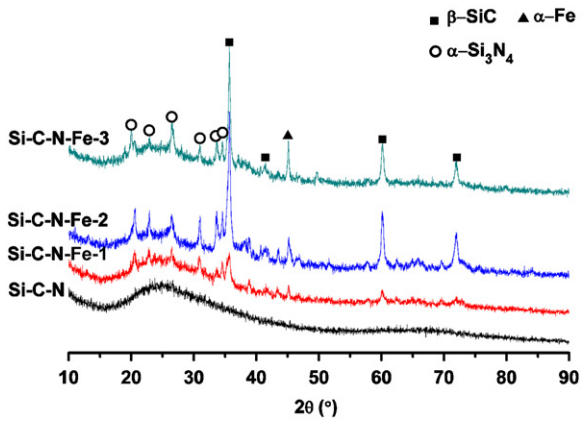

Fig. 8. XRD patterns of 1300 °C ceramic samples with different iron contents.

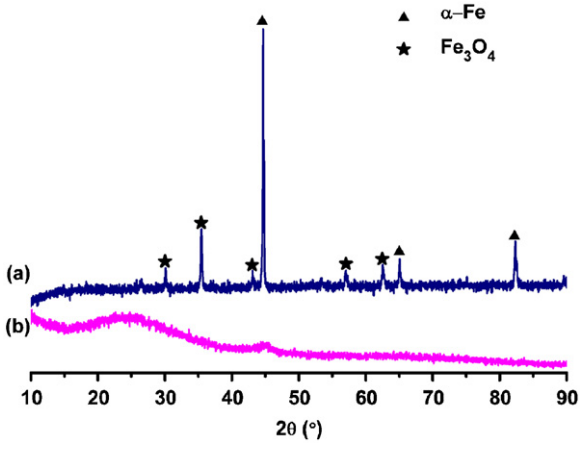

Fig. 9. XRD patterns of (a) $Fe(acac)_3$-derived product and (b) Si–C–N–Fe–3 prepared at 900 °C.

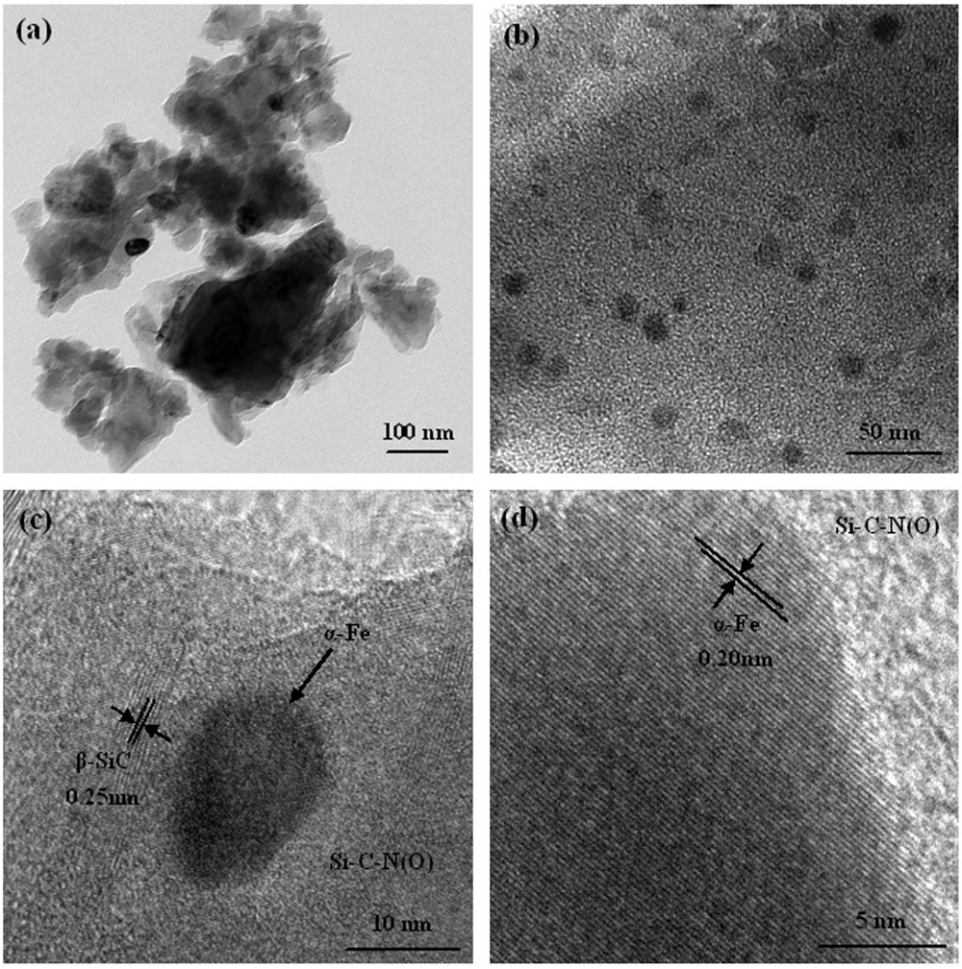

Fig. 10. (a) Bright field lattice image, (b) low- and (c, d) high-resolution transmission electron microscopy images of 1200 °C Si–C–N–Fe–3 ceramic.

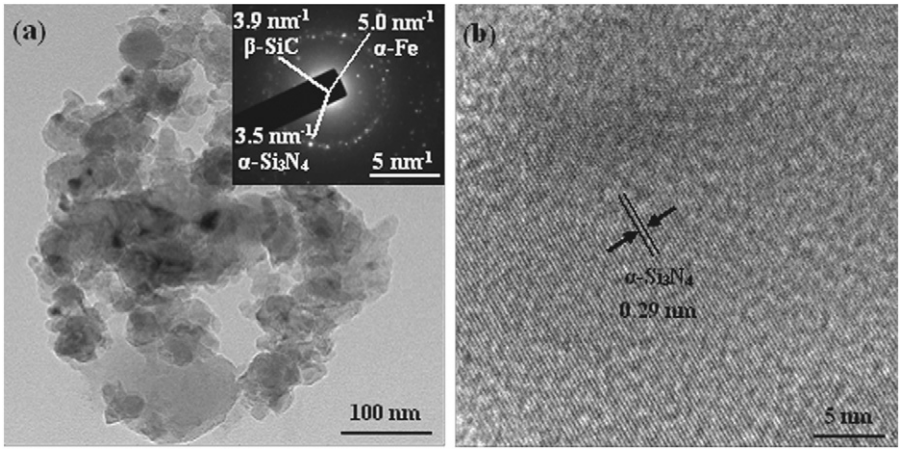

Fig. 11. (a) Bright field lattice image and (b) high-resolution transmission electron microscopy images of 1300 °C Si–C–N–Fe–3 ceramic.

1200 °C ceramic. In the 1300 °C ceramic matrix, the β-SiC, α-Fe and α-Si_3N_4 grains are observed. Fig. 11(b) reveals that the interplanar spacing of 0.29 nm corresponds to the (2 0 1) plane of the α-Si_3N_4 [30], indicating the existence of the α-Si_3N_4 grains. The TEM results are consistent with the XRD measurements.

3.4. Magnetic properties of PFSZ-derived ceramics

Based on the XRD and TEM measurements, the α-Fe is the only magnetic crystalline embedded in the amorphous Si–C–N(O) matrix, which might endow the Si–C–N–Fe system with special magnetic properties. The magnetization behavior

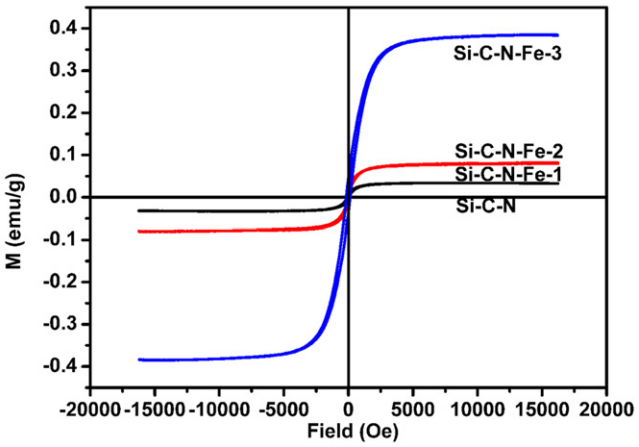

Fig. 12. Magnetization versus applied magnetic field for 1200 °C Si–C–N and Si–C–N–Fe ceramics.

of the Si–C–N–Fe ceramic was thus investigated by the vibration sample magnetometer system. Fig. 12 shows the magnetization curves of the 1200 °C ceramics. All the Si–C–N–Fe ceramics are magnetizable, while the Si–C–N is not. Their magnetization increases rapidly with the increase of the Fe content in the ceramic. The Si–C–N–Fe samples exhibit hysteresis loops. However, their remanent magnetization M_r (<0.1 emu/g) and coercivity H_c (~ 150 Oe) are very low, suggesting that the ceramics are basically soft magnetic materials. Moreover, the magnetic properties of the Si–C–N–Fe ceramic could be easily controlled by the amount of Fe content in the ceramic.

4. Conclusions

In this work, a series of PFSZ precursors were prepared via a condensation reaction between PSZ and $Fe(acac)_3$. The as-synthesized PFSZs were cured and then pyrolyzed to prepare Si–C–N–Fe ceramics. The ceramic yield of the PFSZ was significantly improved by the introduction of $Fe(acac)_3$. In the Si–C–N–Fe system, the α-Fe crystallites were detected in the 900 °C ceramic. Further heating at 1200 °C induced partial crystallization to give mixed XRD patterns for SiC, Si_3N_4, and α-Fe. Moreover, the α-Fe nanoparticles are uniformly dispersed in the amorphous Si–C–N(O) matrix, which might be responsible for the soft magnetization of the resultant Si–C–N–Fe ceramics. The iron content and the magnetic properties of the final ceramic could be easily controlled by adjusting the amount of $Fe(acac)_3$ in the precursor.

Acknowledgments

This work was supported by the National Natural Science Foundation of China (Nos. 50802079 and 51072169), and the Natural Science Foundation of Fujian Province of China (Nos. 2011J01330 and 2010J01307).

References

[1] J. Weiss, H.L. Lukas, J. Lorenz, G. Petzow, H. Krieg, Calculation of heterogeneous phase equilibriums in oxide–nitride systems. I. The quaternary system carbon–silicon–nitrogen–oxygen, Calphad 5 (1981) 125–240.
[2] H.J. Seifert, J. Peng, J. Golczewski, F. Aldinger, Phase equilibria of precusor-derived Si–(B–)–C–N ceramics, Applied Organometallic Chemistry 15 (2001) 794–808.
[3] R. Riedel, A. Kienzle, W. Dressler, L. Ruwisch, J. Bill, F. Aldinger, A silicoboron carbonitride ceramic stable to 2000 °C, Nature 382 (1996) 796–798.
[4] P. Colombo, G. Mera, R. Riedel, G.D. Soraru, Polymer-derived ceramics: 40 years of research and innovation in advanced ceramics, Journal of the American Ceramic Society 93 (2010) 1805–1837.
[5] M. Weinmann, T.W. Kamphowe, J. Schuhmacher, K. Müller, F. Aldinger, Design of polymeric Si–B–C–N ceramic precursors for application in fiber-reinforced composite materials, Chemistry of Materials 12 (2000) 2112–2122.
[6] J. Haberecht, R. Nesper, H. Grützmacher, A construction kit for Si–B–C–N ceramic materials based on borazine precursors, Chemistry of Materials 17 (2005) 2340–2347.
[7] S.H. Lee, M. Weinmann, P. Gerstel, F. Aldinger, Extraordinary thermal stability of SiC particulate-reinforced polymer-derived Si–B–C–N composites, Scripta Materialia 59 (2008) 607–610.
[8] M.J. Maclachlan, M. Ginzburg, N. Coombs, T.W. Coyle, N.P. Raju, J.E. Greedan, G.A. Ozin, I. Manners, Shaped ceramics with tunable magnetic properties from metal-containing polymers, Science 287 (2000) 1460–1463.
[9] I. Manners, Putting metals into polymers, Science 294 (2001) 1664–1666.
[10] W.Y. Chan, S.B. Clendenning, A. Berenbaum, A.J. Lough, S. Aouba, H.E. Ruda, I. Manners, Highly metallized polymers: synthesis, characterization, and lithographic patterning of polyferrocenylsilanes with pendant cobalt, molybdenum, and nickel cluster substituents, Journal of the American Chemical Society 127 (2005) 1765–1772.
[11] Q. Sun, J.W.Y. Lam, K. Xu, H. Xu, J.A.K. Cha, P.C.L. Wong, G. Wen, X. Zhang, X. Jing, Nanocluster-containing mesoporous magnetoceramics from hyperbranched organometallic polymer precursors, Chemistry of Materials 12 (2000) 2617–2624.
[12] Q. Sun, K. Xu, H. Peng, R. Zheng, M. Häussler, B.Z. Tang, Hyperbranched organometallic polymers: synthesis and properties of poly(ferrocenylenesilyne)s, Macromolecules 36 (2003) 2309–2320.
[13] Y. Yu, L. An, Y. Chen, D. Yang, Synthesis of SiFeC magnetoceramics from reverse polycarbosilane-based microemulsions, Journal of the American Ceramic Society 93 (2010) 3324–3329.
[14] X. Chen, Z. Su, L. Zhang, M. Tang, Y. Yu, L. Zhang, L. Chen, Iron nanoparticle-containing silicon carbide fibers prepared by pyrolysis of $Fe(CO)_5$-doped polycarbosilane fibers, Journal of the American Ceramic Society 93 (2010) 89–95.
[15] K. Kulbaba, A. Cheng, A. Bartole, S. Greenberg, R. Resendes, N. Coombs, A. Safa-Sefat, J.E. Greedan, H.D.H. Stöver, G.A. Ozin, I. Manners, Polyferrocenylsilane microspheres: synthesis, mechanism of formation, size and charge tunability, electrostatic self-assembly, and pyrolysis to spherical magnetic ceramic particles, Journal of the American Chemical Society 124 (2002) 12522–12534.
[16] L. Friebe, K. Liu, B. Obermeier, S. Petrov, P. Dube, I. Manners, Pyrolysis of polycarbosilanes with pendant nickel clusters: synthesis and characterization of magnetic ceramics containing nickel and nickel silicide nanoparticles, Chemistry of Materials 19 (2007) 2630–2640.
[17] P.A. Storozhenko, G.I. Scherbakova, A.M. Tsirlin, E.K. Florina, Synthesis of nanozirconooligocarbosilanes, Inorganic Materials 42 (2006) 1159–1167.
[18] S.P. Gubin, A.M. Tsirlin, N.A. Popova, E.K. Florina, E.M. Moroz, Clusters in a polymer matrix: IV. Zr- and Ti-containing nanoparticles formed during the transformation of oligosilacarbosilane into poly (carbosilane): structure and interaction with the matrix, Inorganic Materials 37 (2001) 1317–1326.

[19] S.I. Andronenko, A. Leo, I. Stiharu, S.K. Misra, EPR/FMR investigation of Mn-doped SiCN ceramics, Applied Magnetic Resonance 39 (2010) 347–356.
[20] S.I. Andronenko, I. Stiharu, D. Menard, C. Lacroix, S.K. Misra, EPR/FMR, FTIR, X-ray and Raman investigations of Fe-doped SiCN ceramics, Applied Magnetic Resonance 38 (2010) 385–402.
[21] N. Hering, K. Schreiber, R. Riedel, O. Lichtenberger, J. Woltersdorf, Synthesis of polymeric precursors for the formation of nanocrystalline Ti–C–N/amorphous Si–C–N composites, Applied Organometallic Chemistry 15 (2001) 879–886.
[22] T. Schmalz, T. Kraus, M. Günthner, C. Liebscher, U. Glatzel, R. Kempe, G. Motz, Catalytic formation of carbon phases in metal modified, porous polymer derived SiCN ceramics, Carbon 49 (2011) 3065–3072.
[23] A. Saha, S.R. Shah, R. Raj, S.E. Russek, Polymer-derived SiCN composites with magnetic properties, Journal of Materials Research 18 (2003) 2549–2551.
[24] R. Hauser, A. Francis, R. Theismann, R. Riedel, Processing and magnetic properties of metal-containing SiCN ceramic micro- and nano-composites, Journal of Materials Science 43 (2008) 4042–4049.
[25] A. Dumitru, I. Stamatin, A. Morozan, C. Mirea, V. Ciupina, Si–C–N–Fe nanostuctured ceramics from inorganic polymer precursors obtained by plasma polymerization, Material Science and Engineering: C 27 (2007) 1331–1337.
[26] A. Francis, E. Ionescu, C. Fasel, R. Riedel, Crystallization behavior and controlling mechanism of iron-containing Si–C–N ceramics, Inorganic Chemistry 48 (2009) 10078–10083.
[27] Y. Li, Z. Zheng, C. Reng, Z. Zhang, W. Gao, S. Yang, Z. Xie, Preparation of Si–C–N–Fe magnetic ceramics from iron-containing polysilazane, Applied Organometallic Chemistry 17 (2003) 120–126.
[28] J. Li, Z. Zhang, Z. Zheng, L. Guo, G. Xu, Z. Xie, Preparation and magnetic properties of Fe/Si/C/N ceramics derived from a polymeric precursor, Journal of Applied Polymer Science 105 (2007) 1786–1792.
[29] D.F. Shriver, M.A. Drezdzon, in: The Manipulation of Air-Sensitive Compounds, 2nd ed., Wiley, New York, 1986.
[30] R. Li, C. Zhou, L. Yang, S. Li, J. Zhan, Z. Yu, H. Xia, Synthesis and polymer-to-ceramic conversion of tailorable copolysilazanes, Journal of Applied Polymer Science 122 (2010) 1286–1292.
[31] P.A. Stabnikov, N.V. Pervukhina, I.A. Baidina, L.A. Sheludyakova, S.V. Borisov, On the symmetry of iron(III) tris-acetylacetonate crystals, Journal of Structural Chemistry 48 (2007) 186–192.
[32] T. Ishikawa, Y. Kohtoku, K. Kumagawa, Production mechanism of polyzirconocarbosilane using zirconium (IV) acetylacetonate and its conversion of the polymer into inorganic materials, Journal of Materials Science 33 (1998) 161–166.
[33] Y. Iwamoto, W. Völger, E. Kroke, R. Riedel, Crystallization behavior of amorphous silicon carbonitride ceramics derived from organometallic precursors, Journal of the American Ceramic Society 84 (2001) 2170–2178.
[34] Q. Li, X. Yin, L. Feng, Dielectric properties of Si_3N_4–SiCN composite ceramics in X-band, Ceramics International (2012)http://dx.doi.org/10.1016/j.ceramint.2012.03.045.